features of that interval of the data waveform from the coefficient of the quadratic term and the constant term.

The expansion method utilizes the Hermite polynomial $H_m(x)$,[14) 15)] which is defined as

$$H_m(x) = (-1)^m \{E(x)\}^{-1} \frac{d^m E(x)}{dx^m} \quad (1)$$

$$\sum_{x=-a}^{a} \{H_m(x) H_n(x)\} E(x) = 0 \quad (m \neq n) \quad (2)$$

where $E(x)$ is the Gaussian error function

$$E(x) = \exp\left(-\frac{x^2}{2\sigma^2}\right) \quad (3)$$

and the constant a indicates the defined interval. Moreover, x is the variable in the time direction in units of the sampling time interval. If the normalization constant A_m is defined as

$$A_m = \sum_{x=-a}^{a} \{H_m(x)\}^2 E(x) \quad (4)$$

Then

$$\psi_m(x) = \frac{1}{\sqrt{A_m}} H_m(x) \{E(x)\}^{1/2} \quad (5)$$

constitutes an orthonormal function that may be regarded as a weighting of $H_m(x)$ by $E(x)$. The time-series data $f(t)$ centered on time t is approximated. As in Eq. (5), time-series data $f(t)$ is weighted by $E(x)$ to obtain $h(t)$, which is expanded as:

$$h(t+x) = f(t+x) \{E(x)\}^{1/2} \quad (6)$$

When Eq. (6) is expanded using the orthonormal function in Eq. (5), time-series data $f(t)$ can be expanded as:

$$h(t+x) = \sum_{x=-a}^{\infty} a_m(t) \psi_m(x) = \sum_{x=-a}^{\infty} a_m(t) \frac{1}{\sqrt{A_m}} H_m(x) \{E(x)\}^{1/2} \quad (7)$$

with $a_m(t)(m = 0,1,\cdots,\infty)$ as the expansion coefficient obtained from:

$$a_m(t) = \sum_{x=-a}^{a} h(t+x) \ \psi_m(x). \quad (8)$$

From Eqs. (6) and (7), in the vicinity of time t, expansion of the time-series data $f(t)$ can thus be performed by:

$$h(t+x) = \sum_{x=-a}^{a} a_m(t) \frac{H_m(x)}{\sqrt{A_m}}. \quad (9)$$

Thus, as shown in Eq. (1), $H_m(x)$ is a polynomial of degree m and the time-series data $f(t)$ in the vicinity of time t is expanded using this polynomial. Substituting Eqs. (5) and (4) into Eq. (8) yields

$$a_m(t) = \sum_{x=-a}^{a} f(t+x) \frac{H_m(x)}{\sqrt{A_m}} E(x) \quad (10)$$

We can thus obtain the polynomial coefficient $a_m(t)$, which is obtained from the function $W_m(x)$ as

$$W_m(x) = \frac{H_m(x)}{\sqrt{A_m}} E(x) \quad (11)$$

by multiplying and summing the time-series data $f(t)$. $W_m(x)$ is hereafter called the *feature extraction filter*. Figure 2 shows the feature extraction filters used in obtaining the zero-, first-, and second-order polynomial expansion coefficients.

Using the results of the polynomial expansion with the feature extraction filter $W_m(x)$, we can obtain the restoration value $f_e(t)$ for the time-series data at time t by inserting $x = 0$ into Eq. (9).

$$f_e(t) = \sum_{x=-a}^{\infty} a_m(t) \frac{H_m(0)}{\sqrt{A_m}} = \sum_{x=-a}^{\infty} a_m(t) \ W_m(0) \quad (12)$$

The feature extraction filter width $[a,-a]$ is selected on the basis of the curvature at the point that is determined as the feature point. In calculations using Eq. (12), a second-degree polynomial is assumed to be

sufficient for approximating a small data interval and the maximum degree of the polynomial is defined by setting $m = 2$.

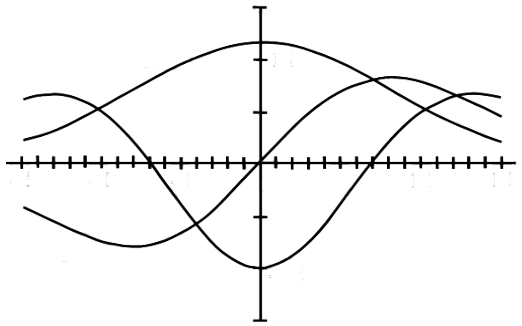

Fig. 2 Feature extraction filter(σ=8) for determining the polynomial expansion coefficient from measured data

2.2.2 Feature extraction method

In Eq. (7), the second-order expansion coefficient $a_2(t)$ represents the time-series curvature in the vicinity of time t. If $a_2(t) > 0$ the curve is convex above and if $a_2(t) < 0$ it is convex below; the larger the value of $|a_2(t)|$ is, the greater its curvature is.

By obtaining the second-order expansion coefficient $a_2(t)$ for time-series data $f(t)$, we can therefore find the "center of balance" of intervals having either a positive or a negative value. The center of balance lies near the point of greatest curvature in the interval and is therefore taken as the feature point time t_j. The method for calculating t_j is illustrated in Fig. 3 for the interval $(t_s,\ t_e)$ having a positive value. As shown, the areas under the curve to the left and right of point t_j are equal and the center of balance t_j lies in the region of maximum height in the waveform peak, which is the point of greatest curvature, and thus close to the feature point. The center of balance is thus taken as the feature point and t_j is obtained from the equation:

$$t_j = \frac{\sum_{t=t_s}^{t=t_e}(t \cdot a_2(t))}{\sum_{t=t_s}^{t=t_e} a_2(t)} \qquad (j = 0,1,\cdots, J) \qquad (13)$$

where t_s is the starting point of a given interval, t_e is its end point, and J is the number of feature points in the time-series data. From the point t_j on the time axis and the restoration point $f_e(t_j)$ obtained from Eq. (12). It is possible to obtain the feature point $(t_j,\ f_e(t_j))$.

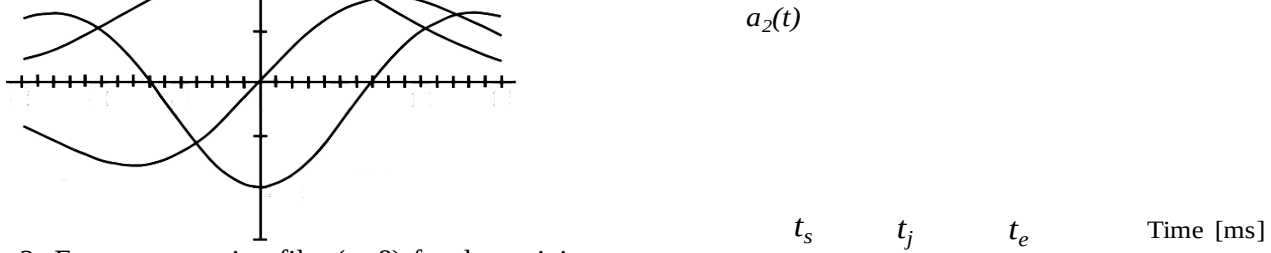

Fig. 3 Location of the center of balance (t_j) is nearest the point of maximum curvature in a positive-value (or negative value) interval ($t_s,\ t_e$) ; hatched and dotted portions are of equal area

2.3 Measured vector series construction

The time-series data restoration point t_j is obtained from Eq. (12) and the corresponding feature point $(t_j, t_e(t_j))$ is calculated. The successive feature points are then connected to express the time-series data $f(t)$ as a vector series:

$$a_j = (t_{j+1} - t_j,\ f_e(t_{j+1}) - f_e(t_j)) \qquad (j = 1,2,\cdots, j-1). \qquad (14)$$

Figure 4 illustrates the course of the polygonal chain approximation of the acoustic data by the vector series. In this example, (a) shows the raw acoustic data, (b) is the smoothed acoustic data obtained by the average movement of each point together with the three points on either side of it, (c) is the second-degree polynomial expansion coefficients $a_2(t)$ calculated with a feature extraction filter having $\sigma = 8$, and (d) is the waveform obtained by the vector series approximation.

2.4 Feature collation

As noted above, DP matching is used to collate and extract the vector series of the range of movement in the region to be diagnosed from the measured vector series. In the collation results, it is necessary to avoid

the correspondence states shown in Fig. 5.

In Fig. 5(a), the third vector from the left in the lower vector series is in redundant correspondence with the second and third vectors in the upper series.

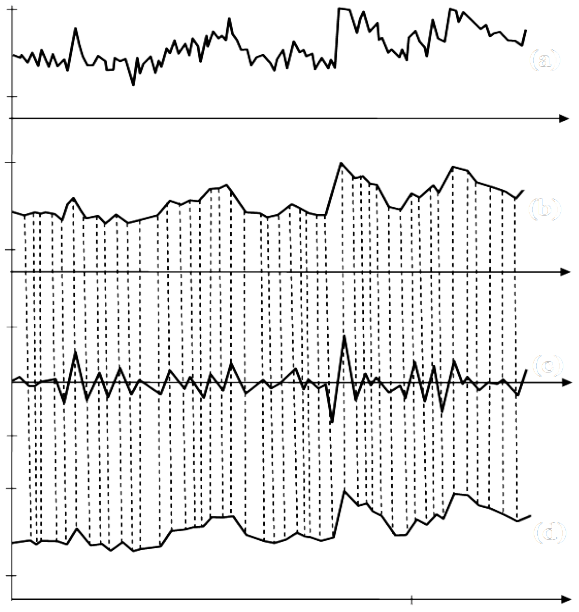

Fig. 4 Acoustic data approximation process:
(a) acoustic data;
(b) mean movement in acoustic data;
(c) second-order coefficient $a_2(t)$ of polynomial expansion (σ=8);
(d) waveform approximated by a vector series.

In Fig. 5(b), the third vector in the lower series does not correspond to any vector in the upper series. To avoid these states at any given node (i, j) and to obtain the route that minimizes the evaluation function value for the two vector series, the route is selected from three directions, as illustrated in Fig. 6.

The evaluation function is applied to route selection at each node (i, j). In the DP matching, during determination of the correspondence for set t in the two vector series, the optimum correspondence of the previous set $t-1$ for minimizing the difference between the two vector series (hereafter referred to as the "error") has already been determined.

When determining the correspondence for set t, at node (i, j), the evaluation function is expressed by:

$$\sum_{c=1}^{t} g_c = \sum_{c=1}^{t-1} g_c + g_t \ , \qquad (15)$$

where g_t is the correspondence error in set t and $\sum_{c=1}^{t-1} g_c$ is the sum of the correspondence errors in sets 1 to $t-1$.

(a) (b)

Fig. 5 Unallowable correspondence between two vector series, where the dotted lines mean the correspondence between vectors.
(a) A vector marked arrow is duplicated by two vectors.
(b) A vector marked arrow has no corresponding vector.

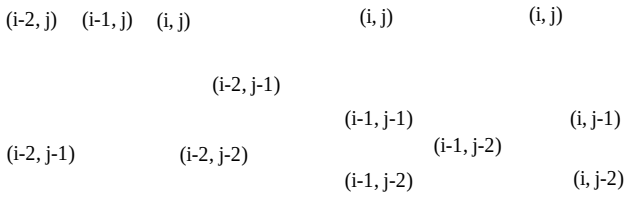

(a) Horizontal Direction (b) Diagonal direction (c) Vertical direction

Fig. 6 Route candidates to the node (i,j)

Error g_t also represents the square of the error between the two vectors. In the correspondence between the two vectors $\boldsymbol{\alpha}$ and $\boldsymbol{\beta}$, this "squared error" can be expressed as:

$$g_t = |\boldsymbol{\alpha} - \boldsymbol{\beta}|^2 = |\boldsymbol{\alpha}|^2 - 2(\boldsymbol{\alpha} \cdot \boldsymbol{\beta}) + |\boldsymbol{\beta}|^2 . \qquad (16)$$

This involves the correspondence of one vector to just one vector and is the case for route (b) in Fig. 6, and would thus lead to its selection. If either route (a) or route (c) were selected, the number of vectors $r(r \geq 1)$ involved in the correspondence to one vector would be larger. In the correspondence of vectors $\boldsymbol{\beta_1} \cdots \boldsymbol{\beta_r}$ to $\boldsymbol{\alpha}$, the squared error may be expressed as:

$$g_t = \left| \boldsymbol{\alpha} - \sum_{p=1}^{r} \boldsymbol{\beta}_p \right|^2$$
$$= |\boldsymbol{\alpha}|^2 - 2\sum_{p=1}^{r} (\boldsymbol{\alpha} \cdot \boldsymbol{\beta}_p) + \left(\sum_{p=1}^{r} |\boldsymbol{\beta}_p| \right)^2 . \quad (17)$$

It should be noted that $\boldsymbol{\beta}_1 \cdots \boldsymbol{\beta}_r$ vector sum in this equation is not $|\boldsymbol{\beta}_1 \cdots \boldsymbol{\beta}_r|$ but rather $|\boldsymbol{\beta}_1| + \cdots + |\boldsymbol{\beta}_r|$.
The former would apply in the case of correspondence to $\boldsymbol{\alpha}$ by a vector extending from the initial point of $\boldsymbol{\beta}_1$ to the terminal point of $\boldsymbol{\beta}_r$. The latter applies for correspondence to $\boldsymbol{\alpha}$ by the vector series $\boldsymbol{\beta}_p (p = 1,2,\cdots,r)$, and the difference between the vector series peak and trough conformations is thus included in the error.

2.5 Abnormality diagnosis

The dissimilarity is calculated for each vector as the correspondence determined by the collation. The dissimilarity is compared with the standard value (the "error limit"), which is established on the basis of the error variation in similar equipment units during normal operation as determined from the frequency distribution of the variations among those units.
When abnormality symptoms begin to appear, changes are generated in the acoustic data waveform. Within the vector series, large changes occur in the slope of the component vectors. Changes in vector length (i.e., shortening or lengthening relative to the time axis) can be attributed in large part to normal fluctuations in acoustic emissions depending on variations in the state of the equipment and other such factors. Accordingly, the change in slope is more strongly represented in quantification of the difference between two corresponding vectors in length and slope as the dissimilarity. For this reason, it is calculated as the product of the squared error and $1-\cos\theta$ (θ: angle between the two vectors). However, a further consideration of vector length is necessary due to the use of DP matching, in which the vector correspondence is not necessarily one to one. Therefore, when correspondence occurs between one vector and $r(r>1)$ vectors, a one-to-one correspondence is constructed by dividing one vector into r parts in accordance with the component time ratios of the other, and the dissimilarities of the vectors in the one-to-one correspondence are then summed. Thus, in the event of correspondence to $\boldsymbol{\alpha}$ by $\boldsymbol{\beta}_1 \cdots \boldsymbol{\beta}_r$, $\boldsymbol{\alpha}$ is divided into $\boldsymbol{\alpha}_1 \cdots \boldsymbol{\alpha}_r$ in accordance with the component time ratios of $\boldsymbol{\beta}_1 \cdots \boldsymbol{\beta}_r$, and the dissimilarity between $\boldsymbol{\alpha}$ and $\boldsymbol{\beta}_1 \cdots \boldsymbol{\beta}_r$ is then obtained as

$$E = \sum_{p=1}^{r} \left\{ (\boldsymbol{\alpha}_q \cdot \boldsymbol{\beta}_q)^2 (1 - \cos\theta_q) \right\}$$
$$\cos\theta_q = (\boldsymbol{\alpha}_q \cdot \boldsymbol{\beta}_q) / (|\boldsymbol{\alpha}_q| |\boldsymbol{\beta}_q|) \quad (18)$$

The enhancement of the increase in dissimilarity with increasing angle between the vectors that results from using the product of the squared error and $1-\cos\theta$ is illustrated by the vector series shown in Figs. 7 and 8. In Fig. 7, the dissimilarity is calculated from the squared error alone, whereas in Fig. 8 it is calculated from the product of the squared error and $1-\cos\theta$. In Fig. 7, large dissimilarities are rather pervasive and the waveform changes are not clearly presented. In Fig. 8, all the dissimilarities are smaller, but those representing differences in the inter-vector angle are much more prominent than those representing differences in vector length, thus more clearly and accurately representing the waveform changes and enabling more reliable detection of the waveform change regions.

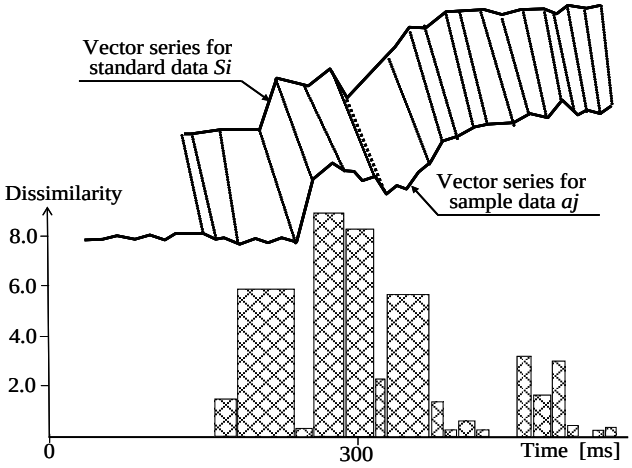

Fig. 7 Dissimilarity between standard vector series and vector series for diagnosis using the squared error

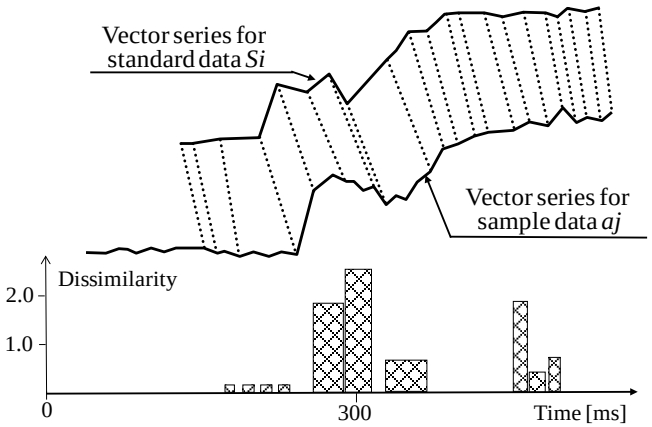

Fig. 8 Dissimilarity between standard vector series and vector series for diagnosis, by product of squared error and (1-cosθ)

3 Experimental results and evaluation

The proposed method described in the previous section was applied experimentally to diagnose the paper-slip transport portion (hereafter called the "transporter") of an actual machine.

The operation of such a transporter during its processing of a slip proceeds in a prescribed sequence, and its acoustic emissions are thus intermittent. During mechanism initialization, operation in the constituent regions of the transporter proceeds in the order determined by an operation verification program. In the evaluation, the acoustic emissions during that time were subjected to a 1/6 octave bandpass filter that passes only 10 kHz, and an envelope was then obtained by squared detection of the resulting output signal. The frequency of 10 kHz was chosen because transporter abnormality is generally most conspicuous at that frequency and 1/6 octave attenuation was used to enable accurate acquisition of the changes in the shape of the waveform. The output signal was sampled at a sampling rate of 1 ms to obtain the time-series data.

In the proposed method, diagnosis of the state of each region within the transporter is performed on the basis of the waveforms of the operating sounds acquired from it in the above-described manner. It is first necessary, however, to establish a standard value as the "error limit", to allow for normal variations among products in a given product line that result in differences among their acoustic data and thus their waveform peak shapes and widths. For this purpose, we measured the acoustic emissions of 84 transporters of the same model during actual operation and determined the resulting error frequency distribution. The term "error" here refers to the divergence between the data from a normally operating transporter and the data from the others. Figure 9 shows the resulting data distribution. The value shown by statistical calculations to be equivalent to a 97% degree of certainty was taken as the standard value. A feature extraction filter having $\sigma = 8$ and a width of 33 $(a = 16)$ was used throughout.

Figure 10 shows typical results of the experimental diagnoses by the proposed method for abnormality detection and Fig. 11 shows results for normal operation. The abnormality in Fig. 10 occurred during paper slip insertion when the paper-slip push plate came into contact with a guide. In the upper half of this figure, (a) and (b) show the standard acoustic data and the acoustic data obtained during the mechanism inspection, respectively. The lower half shows the results obtained by the proposed diagnostic method in the vector correspondence between the two vector series and in dissimilarities between corresponding vectors as shown by the bar graph. A symptom of abnormality is indicated by the circled peak shape in Fig. 10(b), which is absent in Fig. 10(a). In the diagnosis, the dissimilarity in peak shape in the circled portion clearly exceeds the error limit, thus demonstrating the detection of an abnormality. Variations in peak shape can also be observed prior to the circled peak shape, but these represent acoustic emissions just before the start of operation in this region and correspond to ordinary acoustic fluctuations during normal operation. Their dissimilarities, as shown in the bar graph, are smaller than the differences in peak shape that appear in the vector series, due to the use of the method described in Section 2.5 for calculating the dissimilarity. Thus, these results demonstrate the ability of this method for strong representation of vector slope. In contrast to Fig. 10, Fig. 11 shows no difference such as that existing between the circled portions in (a) and (b) of Fig. 10 or any conspicuous dissimilarity such as that in the bar graph in Fig. 10. This demonstrates the ability to detect abnormalities by establishing a standard value.

The proposed method has been applied to the development of a small, practical acoustic diagnosis system containing a digital signal processor (DSP) for rapid performance. The DSP is a single-chip microprocessor specifically designed to process time-series data and other measured values. The system consists of a microphone for acoustic data acquisition and the main unit, which includes a

diagnostic results display and utilizes memory cards that are particularly convenient for storing the necessary data relating to standard vector series and can thus be selected for acoustic diagnosis of different mechanism models and types.

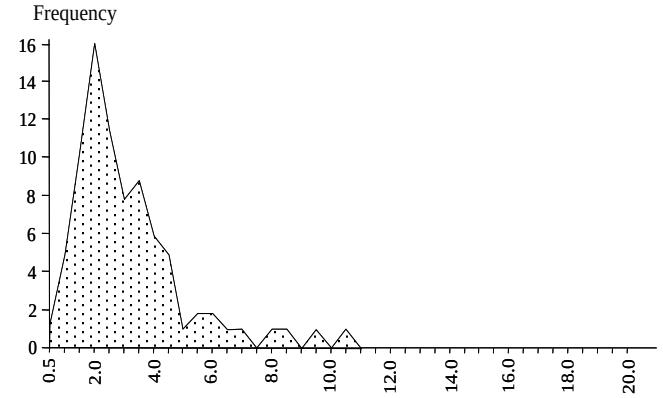

Fig. 9 Error frequency distribution b
84-mechanisms in normal cases

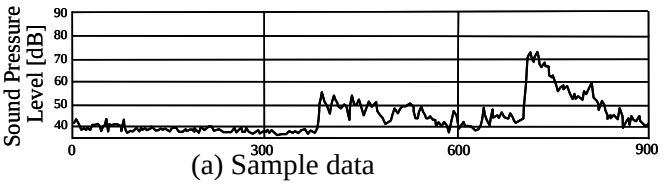

(a) Sample data

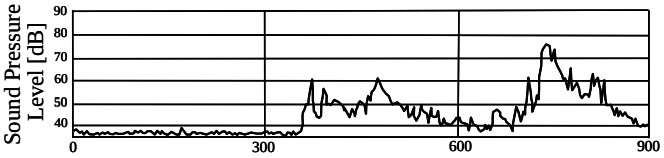

(b) Sample data in the case of fault

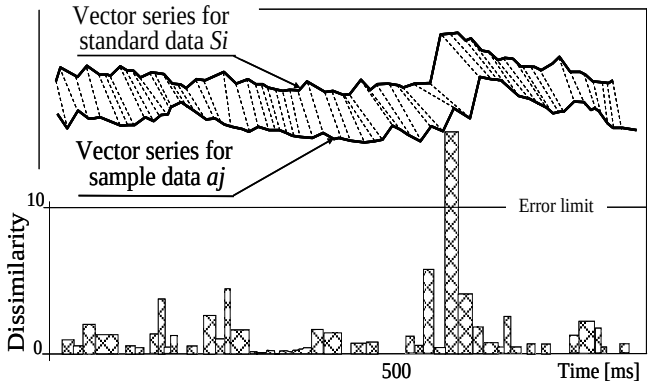

Fig. 10 Diagnosis result in the case of fault

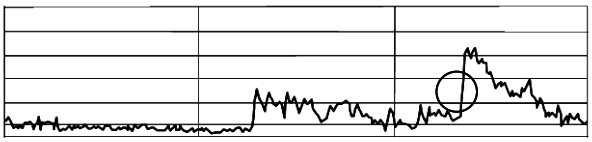

(a) Sample data

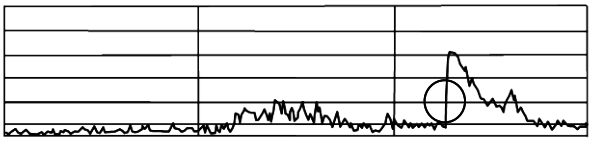

(b) Sample data in the case of ordinary

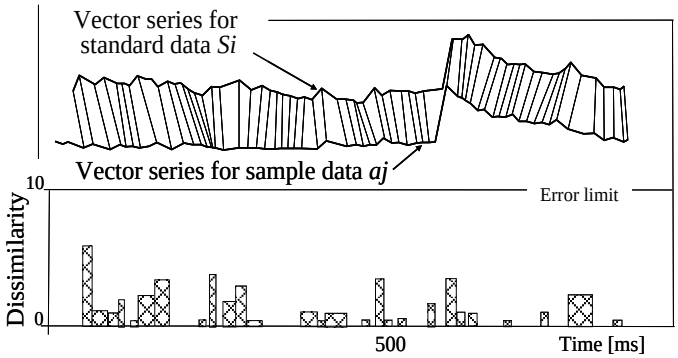

Fig. 11 Diagnosis result in the case of ordinary

4 Conclusions

In this report, we have proposed a technique for diagnosing abnormalities in machines by utilizing their intermittent, episodic sound emissions. We have also described the experimental confirmation of its practicality and effectiveness in which the paper-slip transport region of an actual machine was diagnosed.

This technique includes vector approximation of data-series waveforms, thus eliminating the inordinate processing volume that would be required for acoustic data in the form of raw time-series data and extraction of feature points by a polynomial expansion in which the center of balance is obtained by determining the relevant expansion coefficient. The center of balance in an interval of positive or negative value is near its center of curvature, and is thus taken as the time of the feature point, as described in this report.

It is also necessary to locate the region of the mechanism that is the target of diagnosis despite the occurrence of departures from the time of intermittent sound emission that would apply under the operational sequence prescribed for the various regions, due to the particular state then existing in each region. This

problem of operational asynchronicity, which up to now has posed the greatest impediment to practical acoustic diagnosis of intermittent sound, is eliminated by the proposed method by taking the polygonal approximation of the waveforms of acoustic data during normal operation and during inspection and applying DP matching to collate the two waveform approximations, thereby enabling absorption of the asyncronicities.

We have also described the results of experimental diagnosis of a target region within an actual paper-slip transporter, which confirmed that the technique is effective for acoustic diagnosis. Its facilitation of high-speed calculations with a small memory capacity has enabled the development of a compact diagnostic system containing a single-chip DSP.

In further studies, we intend to investigate its application to other units and to other types of mechanisms.

References:

[1] Cheng-Chien Kuo,Teng-Fa Tsuo, A Novel Defect Classification System of Cost-Resin Transformers by Neural Network under Acoustic Emission Signal, *Proceeding of the 6th WSEAS International Conference on Instrument, Measurement, Circuits & Systems*, 2007, pp.93-98

[2] Gyung-suk Kil, Dae-won Park, Il-kwon Kim, Su-yeon Choi, Analysis of Partial Discharge in Insulation Oil using Acoustic Signal Detection Method, *WSEAS Transactions on Power Systems*, Vol.3, Issue 3, 2008, pp.90-94

[3] A-lan Jiang, Ying-hua Zhao, Li-wei Zhang, Experimental study of acoustic emission characteristics of underwater concrete structures, *IEEE International Symposium on Piezoelectricity, Acoustic Waves, and Device Applications*, 2008, pp.252-257

[4] Ince N.F., Chu-Shu Kao, Kaveh, M., Tewfik, A., Labuz J.F., A-lan Jiang, Ying-hua Zhao, Averaged acoustic emission events for accurate damage localization, *IEEE International Conference on Acoustics, Speech and Signal*, 2009, pp.2201-2204

[5] Dae-won Park, Su-yeon Choi, Gyung-suk Kil, Measurement and Analysis of Acoustic Signal Generated by partial Discharges in Insulation oil, *Proceedings of the 7th WSEAS International Conference on Power System*, 2007, pp.272-275

[6] Zogovic Vukasin, Vukasojevic Radomir, Stojanovic Radovan, Monitoring of the Processed Surface Quality by an Acoustic Emission Application, *Proceedings of the 5th WSEAS International Conference on Signal and Image Processing*, 2005, pp.50-53

[7] Runde M., Ottesen G.E., Skyberg B., Ohlen M., Vibration analysis for diagnostic testing of circuit-breakers, *IEEE Transactions on Power Delivery*, Vol.11, Issue 4, 1996, pp.1816-1823

[8] Xiong Hao, Sun Cai-xin, Artificial Immune Network Classification Algorithm for Fault Diagnosis of Power Transformer, *IEEE Transactions on Power Delivery*, Vol.22, Issue 2, 2007, pp.930-935

[9] Yuying Shao, Zhushi Rao, Zhijian Jin, Online State Diagnosis of Transformer Windings based on Time-frequency Analysis, *WSEAS Transaction on Circuits and Systems*, Vol.8, Issue 2, 2009, pp.227-236

[10] Ciocan R., Ida N., Method of early failure detection for elastic diaphragms based on frequency analysis of the acoustic signal, *IEEE Transactions on Ultrasonics, Ferroelectrics and Frequency Control*, Vol.49, Issue 8, 2002, pp.1025-1028

[11] J. Show, Adaptive Control for Sound and Vibration attenuation: A Comparative study, *Journal of Sound and Vibration*, Vol.235, No.4, 2000, pp.671-684

[12] Bayan N., Erfani S., Frequency Analysis of Time-Varying Systems, *IEEE International Conference on Electro/information Technology*, 2006, pp.33-36

[13] Joo Han Kim, Ha Kyeong Sung, Se Hyun Rhyu, A study on the Vibration Analysis and Test Evaluation for Stack Wheel of Note Handling Units, *IEEE International Electric Machines & Drives Conference*, Vol.2, 2007, pp.1343-1348

[14] Bershad N.J., Celka P., McLaughlin S., Analysis of stochastic gradient identification of Wiener-Hammerstein systems for nonlinearities with Hermite polynomial expansions, *IEEE Transactions on Signal Processing*, Vol.49, Issue 5, 2001, pp.1060-1072

[15] Rao M.M., Sarkar T.K., Adve R.S., Anjali T., Callejon J.F., Extrapolation of electromagnetic responses from conducting objects in time and frequency domain, *IEEE Transactions on Microwave Theory and Techniques*, Vol. 47, Issue 10, 1999, pp. 1964-1974

[16] Ide K., Zhi-Guo Bai, Zi-Jiang Yang, Tsuji, T., Vector approximation method with parameter adaptation and torque control of CSI-fed induction motor, *IEEE Transactions on Industry Applications*, Vol.31, Issue 4, 1995, pp.830-840

[17] Joo Han Kim, Ha Kyeong Sung, Se Hyun Rhyu, A Study on the Natural Frequency Analysis and Test for Note Handling Units, *2nd IEEE Conference on Industrial Electronics and Applications*, 2007, pp.2072-2077

[18] Howe R., Carmichael N.E., JET Engine Test Strategy-program overview and objectives, *IEEE AUTOTESTCON Proceedings*, 2000, pp.284-289

[19] Filippo Neri, Agent based modeling under partial and full knowledge learning settings to simulate financial markets, *AI Communications*, *IOS Press*, 2012, printing